

Exciton dynamics in two-dimensional MoS₂ on a hyperbolic metamaterial-based nanophotonic platform

Kwang Jin Lee,¹ Wei Xin,² Chunhao Fann,¹ Xinli Ma,³ Fei Xing,⁴ Jing Liu,³ Jihua Zhang,¹
Mohamed Elkabbash,¹ and Chunlei Guo^{1,2,*}

¹*The Institute of Optics, University of Rochester, Rochester, New York 14627, USA*

²*GPL, Changchun Institute of Optics, Fine Mechanics and Physics, Chinese Academy of Sciences, Changchun 130033, China*

³*State Key Laboratory of Precision Measurement Technology and Instruments,*

School of Precision Instruments and Opto-electronics Engineering, Tianjin University, Tianjin 300072, China

⁴*School of Physics and Optoelectronic Engineering, Shandong University of Technology, Zibo 255049, China*



(Received 24 May 2019; revised manuscript received 30 August 2019; published 13 January 2020)

The discovery of two-dimensional transition metal dichalcogenides (2D TMDs) has promised next-generation photonics and optoelectronics applications, particularly in the realm of nanophotonics. Arguably, the most crucial fundamental processes in these applications are exciton migration and charge transfer in 2D TMDs. However, exciton dynamics in 2D TMDs has yet to be studied on a nanophotonic platform and, more importantly, the control of exciton dynamics by means of nanophotonic structures still needs to be explored. Here, we demonstrate the control of exciton dynamics in MoS₂ monolayers by introducing a hyperbolic metamaterial (HMM) substrate. We reveal the migration mechanisms of various excitons in MoS₂ monolayers. Furthermore, we experimentally demonstrate that the Förster radius can be increased by HMMs, which is consistent with the theory we developed on the basis of nonlocal effects of HMM. This study will provide a significant step forward in enabling 2D TMD nanophotonic hybrid devices.

DOI: [10.1103/PhysRevB.101.041405](https://doi.org/10.1103/PhysRevB.101.041405)

Following the discovery of graphene, the study of two-dimensional (2D) materials have become one of the most actively pursued areas of research in science and engineering [1–5]. Among them, 2D transition metal dichalcogenides (TMDs) have attracted a great deal of attention and been considered as an ideal material for nanophotonic and optoelectronic applications due to their remarkable optical and electronic properties, such as higher photoluminescence efficiency due to a direct band gap and the existence of light-valley interactions [6–11]. Atomically thin monolayer TMDs have strongly bounded excitons because of the enhancement in quantum confinement and Coulomb interactions, and this strong bonding dominates most optical and electronic effects. In general, the exciton binding energy in TMD monolayers is an order of magnitude higher than that of previously investigated 2D quantum well structures, which leads to their unique optoelectronic characteristics and makes TMDs an ideal platform for exploring exciton dynamics (ED) that is essential for photocurrent conversion processes and novel optoelectronic applications [12,13]. An analog can be seen in organic semiconductors, which also have large exciton binding energies due to their low dielectric constants, and this effect has incited a large amount of exciton dynamics studies in organic photovoltaic operations [14–17]. Therefore, a thorough characterization of ED is of paramount importance for improving light-harvesting applications as well as revealing the fundamental mechanism of the carrier dynamics in 2D

TMDs. More importantly, controlling the ED in these materials is crucial in developing different optoelectronic devices. Although various excitonic properties including ED, exciton lifetime, and exciton band structures in 2D TMDs alone have been intensively studied in recent years [18–21], the control of ED in 2D TMDs by using a nanophotonic structure still needs to be explored.

Engineering light-matter interactions has been realized using nanophotonic structures, e.g., metamaterials and engineered materials with tailored optical properties [22–24]. Particularly, metamaterials have been used in optoelectronic devices [25,26], optical sensing [27], plasmonic lasers [28], and Raman spectroscopy [29]. Among various types of metamaterials, hyperbolic metamaterials (HMMs) have been extensively studied over the past few years due to their unusual optical properties from the high-*k* states [30–34]. HMM structures that have been shown to exert nonlocal effects on the photophysical properties of their surrounding environment have recently been reported [35,36], which suggests that the optical properties of 2D TMDs can be drastically altered without modifying the material itself, but instead by incorporating them on a HMM.

MoS₂ monolayers exhibit two typical band-edge excitons, *A* and *B* excitons, resulting from transitions between the conduction band minimum and spin-orbit split valence band maximum near the *K* point. In addition, recent studies observed another exciton, labeled *C* excitons, with a strong and broadband absorption at higher energies. *C*-exciton states are attributed to the band nesting effect, i.e., a transition arising from the maxima in the joint density of states when the

*Corresponding author: guo@optics.rochester.edu

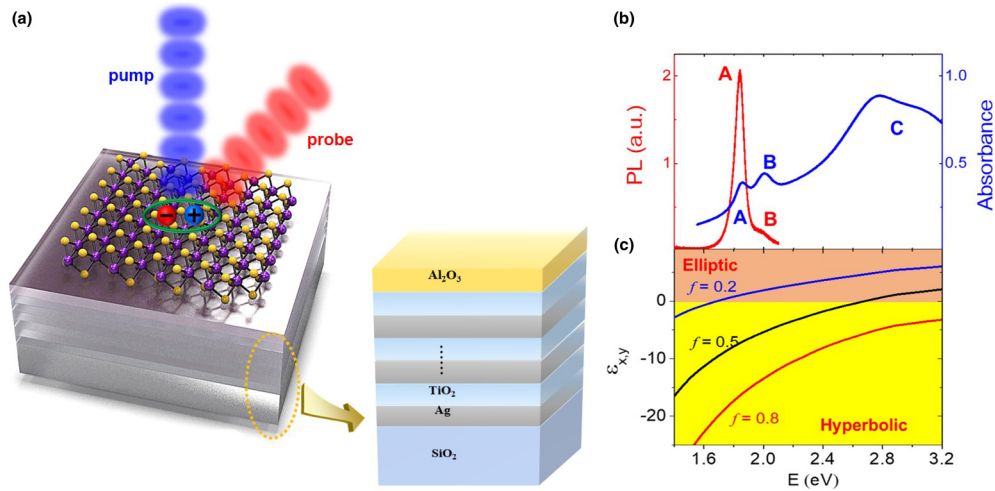


FIG. 1. Sample configuration and characterization. (a) Schematics of the experimental configuration for a MoS₂ monolayer with exciton dynamics based on the transient absorption measurements. The MoS₂ monolayer is deposited on a multilayered HMM structure that consists of five pairs of Ag-TiO₂ layers covered by a Al₂O₃ film to block any charge transport. (b) Absorption and photoluminescence spectra of MoS₂ monolayers with A, B, and C excitons. (c) Real part of the transverse effective dielectric function of HMM for three different fill factors ($f = 0.2, 0.5, 0.8$).

conduction and valence bands are parallel in a region between the K and Γ points [37–41]. Unlike A and B excitons, C excitons have no photoluminescence. Although several studies have attempted to address some aspects of ED in 2D TMDs [42–45], the exact mechanism of exciton migration dynamics still remains unclear. Therefore, a study on controlling the exciton migration process of these materials is still missing.

In this Rapid Communication, we comprehensively study the underlying mechanisms of exciton migration dynamics in 2D MoS₂ and its controllability based on an HMM-based nanophotonic platform. We demonstrate that ED in the A and C excitons shows a very different dynamic process; the migration of the A exciton is mainly through a single-step Förster-type resonance energy transfer (FRET) whereas a multistep diffusion process is responsible for C excitons. We also find that the Förster radius increases in the presence of the HMM substrates in the hyperbolic dispersion region, but the diffusion coefficient is not affected by the HMMs. We elucidate that the increased Förster radius comes from the nonlocal effects of HMMs from the Purcell effect. We note there have been ongoing debates in understanding FRET in complex photonic environments [46], and this study provides conclusive evidence to address these issues.

A MoS₂ monolayer was prepared on silicon substrates by means of chemical vapor deposition. Single-layer samples were identified by optical microscopy and a photoluminescence map shown in Fig. S1 in the Supplemental Material [47]. Multilayered HMMs consisting of five pairs of alternative Ag-TiO₂ layers with different fill factors ($f = 0.2, 0.5, \text{ and } 0.8$) were fabricated by electron beam evaporation. Detailed sample configurations are described in Fig. S2 [47]. We confirmed that the peaks of Raman spectra were not altered with HMM substrates (Fig. S3). In our design, a 10-nm-thick Al₂O₃ layer was deposited on top of the stack to avoid the convolution of other processes such as charge transport between MoS₂ and HMMs (Fig. S4). Figure 1(a) schematically displays the sample configuration for a MoS₂

monolayer deposited on a HMM substrate with $f = 0.5$ (10 nm thickness of each layer). To observe the ED, we used the exciton-exciton annihilation (EEA) method by performing an ultrafast transient absorption (TA) experiment based on the pump-probe technique described below. Figure 1(b) shows the absorption and photoluminescence spectra of the MoS₂ monolayer. The two absorption peaks at 1.87 and 2.05 eV correspond to A and B excitons of the MoS₂ monolayers, respectively. The broad absorption band above 2.80 eV corresponds to the nonemissive C excitons. The photoluminescence peak and shoulder at 1.84 and 2.01 eV correspond to A and B excitons, respectively. Figure 1(c) presents the real part of an effective dielectric constant of HMMs along the transverse direction calculated by the effective medium theory. HMM with $f = 0.8$ ($f = 0.2$) shows hyperbolic (elliptic) dispersion regions for both A and C excitons, whereas HMM with $f = 0.5$ exhibits hyperbolic (elliptic) dispersion for A (C) excitons.

Ultrafast TA experiments were carried out to analyze the ED of MoS₂ monolayers by measuring the relative reflection ($\Delta R/R$). The pump beam at 2.25 eV (3.05 eV) and probe beam at 1.85 eV (3.05 eV) were chosen for A (C) excitons. The pump fluences for the A and C excitons were adjusted to obtain the same initial exciton densities (n_0) immediately after the excitation by the pump. We note that the TA signal of Si is negligible compared to the TA signal of 2D MoS₂ at the frequency range of interest. This allows us to obtain the pure TA signal of MoS₂ by subtracting the TA signal of the Si substrate from the entire TA signal (Fig. S5). Figures 2(a) and 2(b) show the normalized TA kinetics of A and C excitons in the MoS₂ monolayer on a Si substrate without metamaterials for different exciton densities. At the lowest initial exciton density ($n_0 = 0.06 \times 10^{12} \text{ cm}^{-2}$), the TA kinetics for both A and C excitons are fitted by mono-exponential decay functions with characteristic times (τ) of about 186 and 213 ps, corresponding to the intrinsic exciton lifetimes. C excitons have a relatively longer lifetime than A excitons, and this is consistent with previous works showing

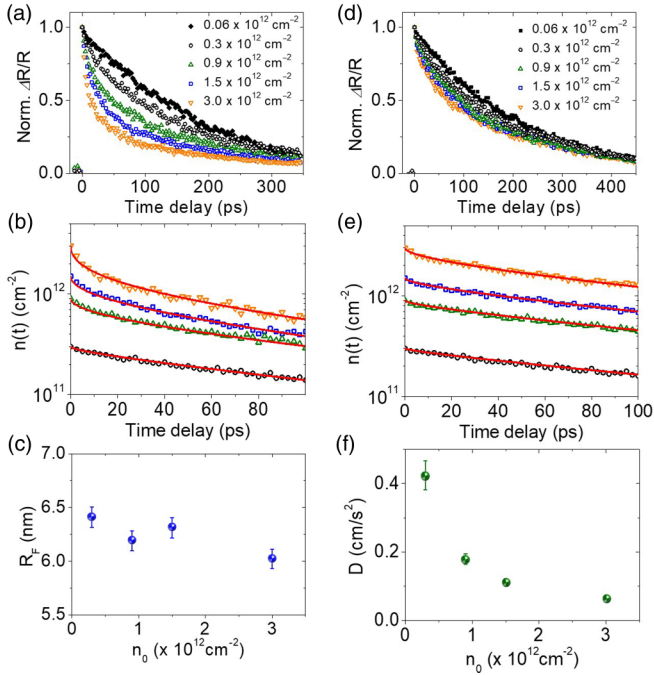


FIG. 2. Transient absorption decays and fitting curves based on exciton-exciton annihilation. (a)–(c) A excitons. (d)–(f) C excitons. (a), (d) Normalized transient absorption decay of A and C excitons, respectively, for several initial exciton densities. (b), (e) Exciton decays for A and C excitons, respectively, in the initial time range (up to 100 ps) with fitting curves based on Eq. (2). (c), (f) Forster radii and the diffusion coefficients for A and C excitons with initial exciton density n_0 .

that favorable band alignment and a transient excited state Coulomb environment could lead to a longer lifetime of C excitons [37,40]. The lifetime of A excitons based on TA measurements ($\tau = 186$ ps) is similar to the emission lifetime obtained by time-resolved photoluminescence measurements ($\tau_{PL} = 175$ ps) as shown in Fig. S6 [47]. As n_0 increases, the decay of A excitons deviates from a monoexponential fitting due to an EEA taking place where two excitons are sufficiently close to interact and to generate a single exciton with a higher energy. Using a biexponential decay fitting, we found that the short time constant (τ_1) decreases with n_0 . On the other hand, the longer time constant (τ_2) is almost independent of n_0 , indicating that τ_1 represents the EEA phenomenon and τ_2 corresponds to the intrinsic exciton lifetime (Fig. S7). For the C exciton, we observed a relatively weak dependence on n_0 , which is also consistent with previous work suggesting that the exciton dissociation occurs efficiently, in agreement with the self-separation of photocarriers in the nesting region in the momentum space [41]. In addition, for A excitons, we note that Fig. 2(a) is consistent with a previous study [42].

Figures 2(c) and 2(d) display the TA decays for A and C excitons in the initial time range (up to ~ 100 ps). To analyze the EEA behavior, we consider the rate equation of EEA described by [48,49]

$$\frac{d}{dt}n(t) = -\frac{n(t)}{\tau} - \frac{1}{2}\gamma(t)n(t)^2, \quad (1)$$

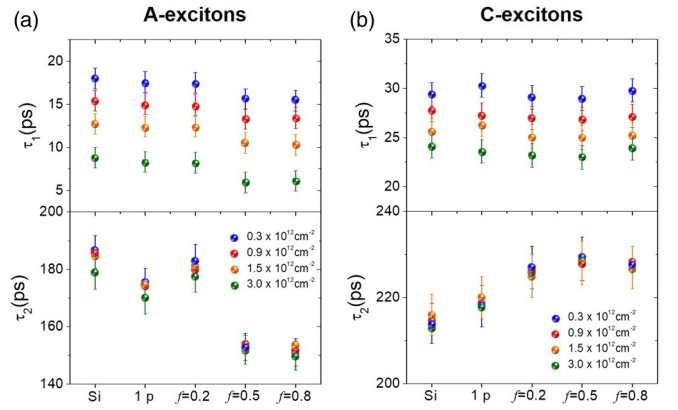


FIG. 3. Behaviors of time constants for A and C excitons with different substrates. (a) Short (τ_1) and long (τ_2) characteristic time constants of A excitons with different substrates for several initial exciton densities. (b) Short (τ_1) and long (τ_2) characteristic time constants of C excitons with different substrates for several initial exciton densities.

where $n(t)$ is the exciton density at a delay time t after the excitation, $\gamma(t)$ is the annihilation rate coefficient, and τ is the intrinsic exciton lifetime at the low exciton density limit (τ_2). The factor $1/2$ represents that only one exciton is left after EEA. We note that EEA is dominant over the Auger recombination in this structure [39]. In general, the EEA process can be classified as two different mechanisms: multistep exciton diffusions and a single-step FRET [48,49]. The exciton diffusion model assumes that the excitons move in a random walk in many steps towards each other before the annihilation takes place. On the other hand, the FRET model considers that annihilation occurs directly via long-range energy transfer processes. FRET strongly depends on the overlap between the emission spectrum of the donor and the absorption spectrum of the acceptor. Here, the FRET process between two identical excitons can depend on a spectral overlap between the exciton emission and the excited state absorption, which is the absorption from the first exciton state to higher electronic states.

For MoS₂ monolayers, we only need to consider FRET and 1D exciton diffusion mechanisms. $\gamma(t)$ is given by $\alpha t^{-1/2}$, where $\alpha = R_F^2 \pi^{3/2} / 2\tau^{1/2}$ for the FRET model with R_F the Förster radius and $\alpha = (8D/\pi)^{1/2} / aN_0$ for the 1D diffusion model with the diffusion coefficient D , lattice constant a , and molecular density N_0 . From these relations, Eq. (1) can be solved as [48,49]

$$n(t) = \frac{n_0 e^{-t/\tau}}{1 + \beta \operatorname{erf}\left(\sqrt{\frac{t}{\tau}}\right)}, \quad (2)$$

where erf is the error function. The coefficient β is expressed by $n_0 R_F^2 \pi^2 / 4$ and $n_0 l_D / aN_0$ for FRET and the 1D diffusion process, respectively. l_D is the diffusion length defined as $(2D\tau)^{1/2}$ (see Supplemental Material Sec. II) The a and N_0 of MoS₂ monolayers were taken as 3.16 Å and 5.7×10^{14} cm⁻², respectively. Here, it is worth noting that $n(t)$ for both the FRET and 1D exciton diffusion models have the same mathematical structure. We have also considered 2D and 3D exciton

diffusion models and fit the experimental results of *C*-exciton density kinetics with the 2D model. Figure S8 [47] shows that the best fit was obtained using the 1D exciton diffusion model, indicating that the diffusion coefficient of *C* excitons is strongly anisotropic and thus allows effective diffusion only along one dimension in a 2D MoS₂ (see Supplemental Material Sec. III; see also Ref. [50] therein).

The solid curves in Figs. 2(b) and 2(e) represent the fits based on Eq. (2). For *C* excitons, FRET was excluded due to their nonemissive property [48]. The diffusion coefficient *D* determined from the fits of the TA decays based on the 1D diffusion model is plotted in Fig. 2(f). Here, the exciton lifetime τ without annihilation was kept as a constant ($\tau = 213$ ps) and thus was not a fitting parameter.

For the *A* exciton, the spectral overlap between the emission and the excited state absorption and the decreasing behavior of τ_1 with n_0 (the quenching effect of the donor exciton) clearly shows that FRET is likely the main mechanism of *A*-exciton migration. Therefore, we plot the R_F as a function of n_0 for the *A* exciton in Fig. 2(e). We find that the value of R_F is around 6.0–6.4 nm and is hardly dependent on n_0 , which is also consistent with the fact that R_F does not depend on the exciton density [Eq. (S8) in the Supplemental Material].

Figure 3 shows the behavior of time constants with different substrates. We note that τ_1 and τ_2 remain constant for all substrates with no overlapping hyperbolic dispersion, while a discernible decrease in τ_1 and τ_2 is observed for HMM with $f = 0.5$ and 0.8 . For *A* excitons, the decrease of τ_2 from 186 to 150 ps can be easily understood in terms of the Purcell factor enhancement based on the high local density of optical states provided by HMMs. Here, we obtain a Purcell factor of ~ 1.24 from the basic relationship given by $\tau_2^{\text{Si}}/\tau_2^{\text{HMM}}$ (Table S1). Interestingly, a shortening of τ_1 due to the hyperbolic dispersion indicates that the nonlocal effect of HMM based on the Purcell factor enhancement clearly affects ED occurring through FRET. The 1*p* substrate consisting of a single pair of 10-nm-thick Ag/TiO₂ films with a 10-nm Al₂O₃ layer on top serves as a control sample showing the relatively unmodified decay kinetics of MoS₂. For *C* excitons, while τ_1 appears to be independent of the substrates, we observed an increase in τ_2 within experimental error. The increase in τ_2 is somewhat similar to the increase in the charge recombination time with the HMM substrates observed in previous studies [35]. All the TA data were plotted in Fig. S9 [47]. We note that the pump fluence was adjusted to obtain the same n_0 by taking the field intensity variation into account in the presence of the HMM structure (Fig. S10).

In Figs. 4(a) and 4(b), we plot R_F and *D* as functions of n_0 for Si and HMM with $f = 0.2$ and 0.8 substrates, respectively. We note that the experimental results for HMM with $f = 0.5$ are almost identical to those for HMM with $f = 0.8$. Figure 4(a) exhibits an enhancement in R_F for the *A* excitons in the HMM hyperbolic dispersion regimes. We can explain this interesting result in terms of the nonlocal effect of HMMs based on the Purcell factor enhancement. It has been shown previously that the nonlocal effect of HMMs could lead to a decrease in the refractive index of the environment effectively [36]. Here, we can equalize the problem as the emitter is placed in a homogenous medium with modified *n*. Based on this discussion, we showed that the Purcell factor is inversely

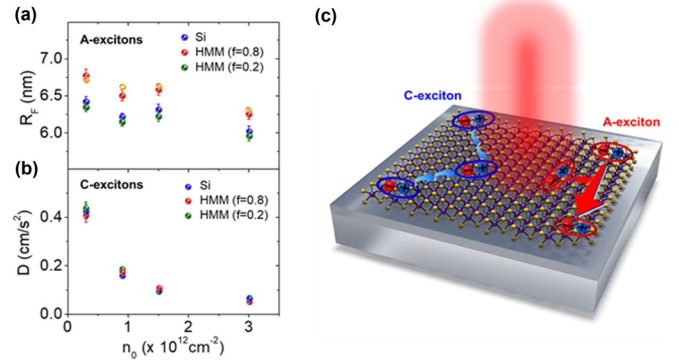


FIG. 4. Underlying mechanism for exciton dynamics and behaviors of the (a) Förster radius (R_F) for *A* excitons and (b) diffusion coefficient (*D*) for *C* excitons as a function of the initial exciton density on different substrates (Si, HMM with $f = 0.2$ and 0.8). (c) Schematics describing the migration mechanisms for *A* and *C* excitons.

proportional to n^3 . We also apply this concept to FRET, and we obtained the relationship between R_F and the Purcell factor (denoted as F_p) as follows (Supplemental Material Sec. IV),

$$R_F \propto F_p^{2/9}. \quad (3)$$

This relation presents a quantitative enhancement factor of R_F by 1.05, which is displayed as the open circles in Fig. 4(a). Surprisingly, the predicted values based on the nonlocal effects of HMMs are almost consistent with the experimental values. We note that the current MoS₂-HMM hybrid systems are an ideal platform to investigate the fundamental relationship between FRET and the photonic environment by excluding quenching effects such as donor-HMM coupling and the charge transport between MoS₂ and HMMs. In the case of the diffusion processes, as shown in Fig. 4(b), there is no noticeable change in the presence of HMMs, which can be explained by the fact that diffusion processes are not relevant for light-matter interactions. Figure 4(c) schematically illustrates the dominant migration mechanisms of the *A* and *C* excitons in 2D MoS₂.

Finally, we discuss the influence of the Purcell effect due to HMM on FRET efficiency. We note that the FRET efficiency η_{FRET} strongly depends on the R_F as in the following equation [51],

$$\eta_{\text{FRET}} = \frac{R_F^6}{R_F^6 + r_T^6} = \left[1 + \left(\frac{r_T}{R_F} \right)^6 \right]^{-1}, \quad (4)$$

where r_T is the distance between two molecules. Equation (4) shows that η_{FRET} is strongly dependent on R_F and r_T . We calculate the r_T for each exciton density n_0 , which are 5.77, 8.16, 10.54, and 18.25 nm for 3.0×10^{12} , 1.5×10^{12} , 0.9×10^{12} , and 0.3×10^{12} cm⁻², respectively. On the basis of the values of R_F obtained from Fig. 4(b), we plot η_{FRET} as a function of n_0 in Fig. 5. We clearly see the $\sim 8.3\%$ enhancement of η_{FRET} in the presence of HMM for $n_0 = 3.0 \times 10^{12}$ cm⁻².

In conclusion, based on the different underlying migration mechanisms of *A*- and *C*-exciton dynamics in 2D MoS₂, the

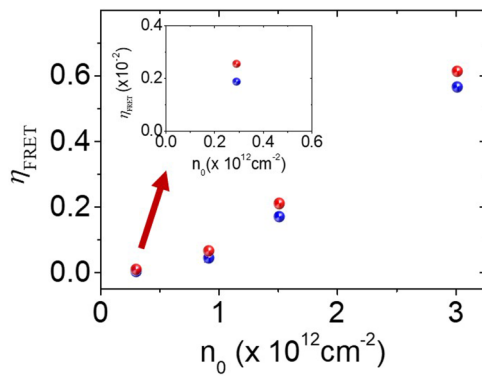


FIG. 5. Plot of FRET efficiency as a function of n_0 in the absence (blue) and presence (red) of HMM. (Inset: Magnification at $n_0 = 0.3 \times 10^{12} \text{ cm}^{-2}$.)

single-step Förster-type resonance energy transfer for the A exciton, and the multistep diffusion process for the C exciton, we investigate the in-depth optical interplay between 2D TMDs and metamaterials by integrating 2D MoS₂ on a

range of nanophotonic platforms using HMMs with different fill factors. We find an increase in the Förster radius for A excitons when the A -exciton spectral region lies in the hyperbolic dispersion region. Furthermore, we develop another theoretical model determining the relationship between the Förster radius and Purcell factor. Our study clearly shows that HMMs can alter the FRET process. There has been a great amount of controversy regarding FRET playing a role in the strength of the excitation interactions in 2D TMDs in the presence of the surrounding media. We resolve this issue by showing that FRET plays the dominant role in the A exciton. Our work presents a way to nanoengineer 2D TMDs with a metamaterial-based nanophotonic platform, which will advance applications of 2D materials in photonics, optoelectronics, and metadvice.

This research was supported by the Bill & Melinda Gates Foundation, National Science Foundation, National Natural Science Foundation (NSFC, Grant No. 11804334), and K.C. Wong Educational Foundation (GJTD-2018-08).

K. J. L. and W. X. contributed equally to this work.

- [1] A. K. Geim and K. S. Novoselov, The rise of graphene, *Nat. Mater.* **6**, 183 (2007).
- [2] F. Bonaccorso, Z. Sun, T. Hasan, and A. C. Ferrari, Graphene photonics and optoelectronics, *Nat. Photonics* **4**, 611 (2010).
- [3] S. Z. Butler, S. M. Hollen, L. Cao, Y. Cui, J. A. Gupta, H. R. Gutierrez, T. F. Heinz, S. S. Hong, J. Huang, A. F. Ismach, E. J. Halperin, M. Kuno, V. V. Plashnitsa, R. D. Robinson, R. S. Ruoff, S. Salahuddin, J. Shan, L. Shi, M. G. Spencer, M. Terrones, W. Windl, and J. E. Goldberger, Progress, challenges, and opportunities in two-dimensional materials beyond graphene, *ACS Nano* **7**, 2898 (2013).
- [4] Q. H. Wang, K. Kalantar-Zadeh, A. Kis, J. N. Coleman, and M. S. Strano, Electronics and optoelectronics of two dimensional transition metal dichalcogenides, *Nat. Nanotechnol.* **7**, 699 (2012).
- [5] W. Xin, X.-K. Li, X.-L. He, B.-W. Su, X.-Q. Jiang, K.-X. Huang, X.-F. Zhou, Z.-B. Liu, and J.-G. Tian, Black-phosphorus-based orientation-induced diodes, *Adv. Mater.* **30**, 1704653 (2017).
- [6] K. F. Mak, C. Lee, J. Hone, J. Shan, and T. F. Heinz, Atomically Thin MoS₂: A New Direct-Gap Semiconductor, *Phys. Rev. Lett.* **105**, 136805 (2010).
- [7] M. Amani, D.-H. Lien, D. Kiriya, J. Xiao, A. Azcatl, J. Noh, S. R. Madhupathy, R. Addou, S. KC, M. Dubey, K. Cho, R. M. Wallace, S.-C. Lee, J.-H. He, J. W. Ager III, X. Zhang, E. Yablonovitch, and A. Javey, Near-unity photoluminescence quantum yield in MoS₂, *Science* **350**, 1065 (2015).
- [8] K. F. Mak and J. Shan, Photonics and optoelectronics of 2D semiconductor transition metal dichalcogenides, *Nat. Photonics* **10**, 216 (2016).
- [9] S. Sampat, T. Guo, K. Zhang, J. A. Robinson, Y. Ghosh, K. P. Acharya, H. Htoon, J. A. Hollingsworth, Y. N. Gartstein, and A. V. Malko, Exciton and trion energy transfer from giant semiconductor nanocrystals to MoS₂ Monolayers, *ACS Photonics* **3**, 708 (2016).
- [10] J. S. Ross, S. Wu, H. Yu, N. J. Ghimire, A. M. Jones, G. Aivazian, J. Yan, D. G. Mandrus, D. Xiao, W. Yao, and X. Xu, Electrical control of neutral and charged excitons in a monolayer semiconductor, *Nat. Commun.* **4**, 1474 (2013).
- [11] K. F. Mak, D. Xiao, and J. Shan, Light-valley interactions in 2D semiconductors, *Nat. Photonics* **12**, 451 (2018).
- [12] M.-L. Tsai, S.-H. Su, J.-K. Chang, D.-S. Tsai, C.-H. Chen, C.-I. Wu, L.-J. Li, L.-J. Chen, and J. H. He, Monolayer MoS₂ heterojunction solar cells, *ACS Nano* **8**, 8317 (2014).
- [13] E. Singh, K. S. Kim, G. Y. Yeom, and H. S. Nalwa, Atomically thin-layered molybdenum disulfide (MoS₂) for bulk-heterojunction solar cells, *ACS Appl. Mater. Interfaces* **9**, 3223 (2017).
- [14] L. Yuan, T. Wang, T. Zhu, M. Zhou, and L. Huang, Exciton dynamics, transport, and annihilation in atomically thin two-dimensional semiconductors, *J. Phys. Chem. Lett.* **8**, 3371 (2017).
- [15] Y. Tamai, H. Ohkita, H. Bente, and S. Ito, Exciton diffusion in conjugated polymers: From fundamental understanding to improvement in photovoltaic conversion efficiency, *J. Phys. Chem. Lett.* **6**, 3417 (2015).
- [16] M. S. Matthew, W. A. Luhman, and R. J. Holmes, Tailored exciton diffusion in organic photovoltaic cells for enhanced power conversion efficiency, *Nat. Mater.* **12**, 152 (2013).
- [17] J. D. A. Lin, O. V. Mikhnenko, J. Chen, Z. Masri, A. Ruseckas, A. Mikhailovsky, R. P. Raab, J. Liu, P. W. M. Blom, M. A. Loi, C. J. Garcia-Cervera, I. D. W. Samuel, and T.-Q. Nguyen, Systematic study of exciton diffusion length in organic semiconductors by six experimental methods, *Mater. Horiz.* **1**, 280 (2014).
- [18] Y. Yu, Y. Yu, C. Xu, A. Barrette, K. Gundogdu, and L. Cao, Fundamental limits of exciton-exciton annihilation for light emission in transition metal dichalcogenide monolayers, *Phys. Rev. B* **93**, 201111(R) (2016).

- [19] T. Kato and T. Kaneko, Transport dynamics of neutral excitons and trions in monolayer WS₂, *ACS Nano* **10**, 9687 (2016).
- [20] M. Palummo, M. Bernardi, and J. C. Grossman, Exciton radiative lifetimes in two-dimensional transition metal dichalcogenides, *Nano Lett.* **15**, 2794 (2015).
- [21] F. Wu, F. Qu, and A. H. MacDonald, Exciton band structure of monolayer MoS₂, *Phys. Rev. B* **91**, 075310 (2015).
- [22] J. B. Pendry, Negative Refraction Makes a Perfect Lens, *Phys. Rev. Lett.* **85**, 3966 (2000).
- [23] R. Maas, J. Parsons, N. Engheta, and A. Polman, Experimental realization of an epsilon-near-zero metamaterial at visible wavelengths, *Nat. Photonics* **7**, 907 (2013).
- [24] N. Yu and F. Capasso, Flat optics with designer metasurfaces, *Nat. Mater.* **13**, 139 (2014).
- [25] M. Esfandyarpour, E. C. Garnett, Y. Cui, M. D. McGehee, and M. L. Brongersma, Metamaterial mirrors in optoelectronic devices, *Nat. Nanotechnol.* **9**, 542 (2014).
- [26] H. Choi, S.-J. Ko, Y. Choi, P. Joo, T. Kim, B. R. Lee, J.-W. Jung, H. J. Choi, M. Cha, J.-R. Jeong, I.-W. Hwang, M. H. Song, B.-S. Kim, and J. Y. Kim, Versatile surface plasmon resonance of carbon-dot-supported silver nanoparticles in polymer optoelectronic devices, *Nat. Photonics* **7**, 732 (2013).
- [27] H. Hodaei, A. U. Hassan, S. Wittek, H. Garcia-Gracia, R. El-Ganainy, D. N. Christodoulides, and M. Khajavikhan, Enhanced sensitivity at higher-order exceptional points, *Nature (London)* **548**, 187 (2017).
- [28] J. B. Khurgin and G. Sun, Comparative analysis of spasers, vertical-cavity surface-emitting lasers and surface-plasmon-emitting diodes, *Nat. Photonics* **8**, 468 (2014).
- [29] R. Zhang, Y. Zhang, Z. C. Dong, S. Jiang, C. Zhang, L. G. Chen, L. Zhang, Y. Liao, J. Aizpurua, Y. Luo, J. L. Yang, and J. G. Hou, Chemical mapping of a single molecule by plasmon-enhanced Raman scattering, *Nature (London)* **498**, 82 (2013).
- [30] H. N. S. Krishnamoorthy, Z. Jacob, E. Narimanov, I. Kretzschmar, and V. M. Menon, Topological transitions in metamaterials, *Science* **336**, 205 (2012).
- [31] A. Poddubny, I. Iorsh, P. Belov, and Y. Kivshar, Hyperbolic metamaterials, *Nat. Photonics* **7**, 948 (2013).
- [32] D. Lu, J. J. Kan, E. E. Fullerton, and Z. Liu, Enhancing spontaneous emission rates of molecules using nanopatterned multilayer hyperbolic metamaterials, *Nat. Nanotechnol.* **9**, 48 (2014).
- [33] T. Tumkur, G. Zhu, P. Black, Y. A. Barnakov, C. E. Bonner, and M. A. Noginov, Control of spontaneous emission in a volume of functionalized hyperbolic metamaterial, *Appl. Phys. Lett.* **99**, 151115 (2011).
- [34] K. J. Lee, Y. U. Lee, S. J. Kim, and P. André, Hyperbolic dispersion dominant regime identified through spontaneous emission variations near metamaterial interfaces, *Adv. Mater. Interfaces* **5**, 1701629 (2018).
- [35] K. J. Lee, Y. Xiao, J. H. Woo, E. Kim, D. Kreher, A.-J. Attias, F. Mathevet, J.-C. Ribierre, J. W. Wu, and P. André, Charge-transfer dynamics and nonlocal dielectric permittivity tuned with metamaterial structures as solvent analogues, *Nat. Mater.* **16**, 722 (2017).
- [36] K. J. Lee, Y. U. Lee, F. Fages, J.-C. Ribierre, J. W. Wu, and A. D'Aléo, Blue-shifting intramolecular charge transfer emission by nonlocal effect of hyperbolic metamaterials, *Nano Lett.* **18**, 1476 (2018).
- [37] S. H. Aleithan, M. Y. Livshits, S. Khadka, Jeffrey J. Rack, M. E. Kordesch, and E. Stinaff, Broadband femtosecond transient absorption spectroscopy for a CVD MoS₂ monolayer, *Phys. Rev. B* **94**, 035445 (2016).
- [38] A. Carvalho, R. M. Ribeiro, and A. H. Castro Neto, Band nesting and the optical response of two-dimensional semiconducting transition metal dichalcogenides, *Phys. Rev. B* **88**, 115205 (2013).
- [39] D. Kozawa, R. Kumar, A. Carvalho, K. K. Amara, W. Zhao, S. Wang, M. Toh, R. M. Ribeiro, A. H. Castro Neto, K. Matsuda, and G. Eda, Photocarrier relaxation pathway in two-dimensional semiconducting transition metal dichalcogenides, *Nat. Commun.* **5**, 4543 (2014).
- [40] L. Wang, Z. Wang, H.-Y. Wang, G. Grinblat, Y.-L. Huang, D. Wang, X.-H. Ye, X.-B. Li, Q. Bao, A.-S. Wee, S. A. Maier, Q.-D. Chen, M.-L. Zhong, C.-W. Qiu, and H.-B. Sun, Slow cooling and efficient extraction of C-exciton hot carriers in MoS₂ monolayer, *Nat. Commun.* **8**, 13906 (2016).
- [41] W. Li, A. G. Birdwell, M. Amani, R. A. Burke, X. Ling, Y.-H. Lee, X. Liang, L. Peng, C. A. Richter, J. Kong, D. J. Gundlach, and N. V. Nguyen, Broadband optical properties of large-area monolayer CVD molybdenum disulfide, *Phys. Rev. B* **90**, 195434 (2014).
- [42] D. Sun, Y. Rao, G. A. Reider, G. Chen, Y. You, L. Brézin, A. R. Harutyunyan, and T. F. Heinz, Observation of rapid exciton-exciton annihilation in monolayer molybdenum disulfide, *Nano Lett.* **14**, 5625 (2014).
- [43] N. Kumar, Q. Cui, F. Ceballos, D. He, Y. Wang, and H. Zhao, Exciton-exciton annihilation in MoSe₂ monolayers, *Phys. Rev. B* **89**, 125427 (2014).
- [44] L. Yuan and L. Huang, Exciton dynamics and annihilation in WS₂ 2D semiconductors, *Nanoscale* **7**, 7402 (2015).
- [45] A. Ghazaryan, M. Hafezi, and P. Ghaemi, Anisotropic exciton transport in transition-metal dichalcogenides, *Phys. Rev. B* **97**, 245411 (2018).
- [46] C. L. Cortes and Z. Jacob, Fundamental figures of merit for engineering Förster resonance energy transfer, *Opt. Express* **26**, 19371 (2018).
- [47] See Supplemental Material at <http://link.aps.org/supplemental/10.1103/PhysRevB.101.041405> for details on the sample preparation and characterizations, and detailed data analyses, which includes Ref. [50].
- [48] E. Engel, K. Leo, and M. Hoffmann, Ultrafast relaxation and exciton-exciton annihilation in PTCDA thin films at high excitation densities, *Chem. Phys.* **325**, 170 (2006).
- [49] H.-Y. Shin, J. H. Woo, M. J. Gwon, M. Barthelemy, M. Vomir, T. Muto, K. Takaishi, M. Uchiyama, D. Hashizume, T. Aoyama, D.-W. Kim, S. Yoon, J.-Y. Bigot, J. W. Wu, and J. C. Ribierre, Exciton diffusion in near-infrared absorbing solution-processed organic thin films, *Phys. Chem. Chem. Phys.* **15**, 2867 (2013).
- [50] Y. Tamai, Y. Matsuura, H. Ohkita, H. Bente, and S. Ito, One-Dimensional Singlet Exciton Diffusion in Poly(3-hexylthiophene) Crystalline Domains, *J. Phys. Chem. Lett.* **5**, 399 (2014).
- [51] M. Lunz, A. L. Bradley, V. A. Gerard, S. J. Byrne, Y. K. Gun'ko, V. Lesnyak, and N. Gaponik, Concentration dependence of Förster resonant energy transfer between donor and acceptor nanocrystal quantum dot layers: Effect of donor-donor interactions, *Phys. Rev. B* **83**, 115423 (2011).